

EXIT Charts Analysis for Turbo-TCM Schemes Using Non-Binary RSC Encoders

Calin Vladeanu, Alexandru Martian
 Telecommunications Department
 University Politehnica of Bucharest
 Bucharest, Romania
 Email: calin@comm.pub.ro

Safwan El Assad
 IETR Laboratory
 UMR CNRS 6164, Image team - site of Nantes
 École d'Ingénieurs de l'Université de Nantes
 Nantes, France
 Email: safwan.elassad@univ-nantes.fr

Abstract—Recently, a new family of recursive systematic convolutional (RSC) encoders over Galois field $\text{GF}(2^N)$ was introduced. The present paper considers the parallel turbo trellis coded modulation (TTCM) scheme using these non-binary encoders as constituent codes. Besides operating over a higher order Galois field, these encoders use a non-linear function, the left-circulate (LCIRC) function, to control the encoder states. It is shown that these rate- $(N-1)/N$ $\text{GF}(2^N)$ RSC-LCIRC encoders offer the same performances in terms of minimum Euclidian distance, effective length, and product distance, as compared to corresponding binary encoders. Moreover, these RSC-LCIRC encoders are requiring less memory usage. Extrinsic information transfer (EXIT) charts are used to analyze the convergence of the proposed punctured TTCM schemes, with 8-PSK and 16-QAM modulations, symbol-by-symbol log-MAP decoding algorithm, when transmitting over AWGN and Rayleigh non-selective fading channels. EXIT charts show some improvements in terms of TTCM decoding schemes convergence for the RSC-LCIRC codes as compared to their binary counterparts.

Keywords-EXIT charts; $\text{GF}(2^N)$ encoders; Punctured Turbo TCM; Symbol-by-Symbol log-MAP; LCIRC

I. INTRODUCTION

In the latter years, nonlinear functions proved to be suitable to implement several telecommunications systems blocks, such as pseudo-random number generation, spreading for code-division multiple access systems, and encryption. Among these nonlinear functions the ones operating in finite precision are more suitable for digital implementations. In [1], Frey proposed a nonlinear digital infinite impulse response (IIR) filter for secure communications. The Frey filter contains a nonlinear function named left-circulate function (LCIRC), which provides the chaotic properties of the filter. The above mentioned work considered the Frey encoder as a digital filter, operating over Galois field $\text{GF}(2^N)$. In [2] it was demonstrated that the Frey encoder with finite precision (wordlength of N bits) presented in [1] is a recursive convolutional encoder operating over $\text{GF}(2^N)$. New methods for enhancing the performances of the phase shift keying - trellis-coded modulation (PSK-TCM) transmissions over a noisy channel, using the recursive convolutional LCIRC (RC-LCIRC) encoders, were proposed in [3]. These encoders follow the rules proposed by Ungerboeck [4] for defining optimum TCM by proper set partitioning

for channels with additive white Gaussian noise (AWGN). When assuming a Rayleigh non-selective fading channel, other designing criteria can be used to optimize the TCM system performances, such as minimum effective length and product distance [5]. Turbo coded schemes were developed as well for the TCM schemes [6], [7]. A family of nonlinear encoders for turbo TCM (TTCM) scheme was proposed in [8]. The present paper aims to extend the performances analysis for these nonlinear TTCM schemes. The extrinsic information transfer (EXIT) chart is an important tool for visualizing the exchange of the extrinsic information between constituent decoders in a turbo receiver scheme [9]. The EXIT chart was also applied to turbo TCM (TTCM) schemes to depict the decoding trajectory, allowing the prediction of bit error rate (BER) waterfall and BER floor regions [10], [11]. Therefore, the EXIT chart can be used as a tool in the design of TTCM schemes [12].

In the present work, the analysis of the TTCM scheme from [8] is extended by considering also the quadrature amplitude modulation (QAM) and a Rayleigh fading channel. Moreover, the EXIT charts are presented to underline the convergence behavior of these schemes.

The paper is organized as follows. Section II is presenting the recursive systematic convolutional LCIRC (RSC-LCIRC) encoder operating over Galois field $\text{GF}(2^N)$ and the optimum set partitioning for two-dimensional TCM schemes. The minimum Euclidian distance, minimum effective length and product distance are estimated for the AWGN channel, and the Rayleigh fading channel, respectively. In Section III, a parallel TTCM transmission scheme using RSC-LCIRC component encoders with symbol puncturing is presented. A symbol-by-symbol log-MAP algorithm is used for the iterative detection. EXIT charts are plotted in Section IV to compare the convergence of different TTCM decoding schemes for the punctured 8-PSK and 16-QAM TTCM transmissions. Finally, the conclusions are drawn in Section V.

II. OPTIMUM RSC-LCIRC ENCODER FOR TCM SCHEMES

In this section, a new family of RSC encoders operating over Galois field $\text{GF}(2^N)$ and their use for optimum TCM

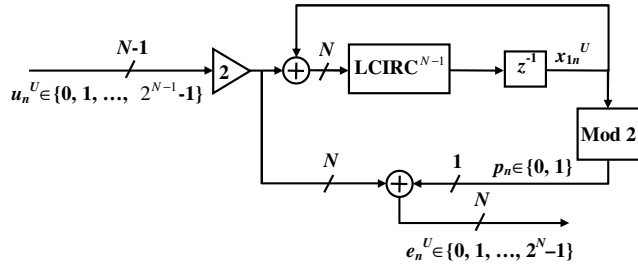


Figure 1. Rate $(N - 1)/N$ optimum $GF(2^N)$ RSC-LCIRC encoder.

schemes are presented. The main component of the RSC encoder presented in the sequel is the nonlinear LCIRC function introduced by Frey in [1] for chaotic encryption. The use of the LCIRC function for channel encoding was considered for the first time in [2]. Optimum encoders using the LCIRC function for TCM schemes were introduced in [3]. However, despite being characterized by optimum Euclidian distances, these recursive convolutional encoders are non-systematic. Therefore, the coding features of these non-systematic encoders are not fully exploited in turbo schemes. In this section, we introduce a new encoder operating over Galois field $GF(2^N)$, using the LCIRC function, which is systematic, i.e., the encoder output value specifies explicitly the input value. Let us denote by N the wordlength used for binary representation of each sample. The LCIRC function performs a bit rotation by placing the most significant bit to the least significant bit, and shifting the other $N - 1$ bits one position to a higher significance.

The block scheme for a rate $(N - 1)/N$ RSC-LCIRC encoder, using one delay element and the LCIRC function is presented in Fig. 1. For each moment n , u_n represents the input data sample, x_{1n} denotes the delay output or the encoder current state, and e_n is the output sample. The superscript U denotes that all the samples are represented in unsigned N bits wordlength, i.e., $u_n^U \in [0, 2^{N-1} - 1]$, $e_n^U \in [0, 2^N - 1]$. The rate for the encoder in Fig. 1 is the ratio between the input wordlength $N_{in} = N - 1$ and the output wordlength N , i.e., $R = N_{in}/N$ [2]. $LCIRC^{N-1}$ represents the LCIRC function application for $N - 1$ times consecutively. Both adders and the multiplier are modulo- 2^N operators. The modulo-2 block extracts the least significant bit, denoted by p_n , from the encoder current state value, x_{1n} . Therefore, p_n is the parity bit for the systematic rate $(N - 1)/N$ encoder. It is important to demonstrate that the encoder is systematic, i.e., the encoder output binary representation codeword e_n^U includes the representation codeword of the encoder input u_n^U . Hence, the output is obtained by shifting the $N - 1$ bits of the input representation codeword by one position to a higher significance, and adding the parity bit p_n to the least significant position, a position that was left empty, inside the N bits output codeword, by the previously mentioned shifting. The one position shifting

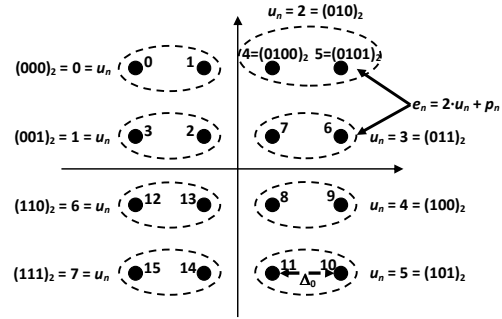


Figure 2. Set partitioning for punctured 16-QAM TCM.

presented above is equivalent to a multiplication by 2 in the $GF(2^N)$ field. Therefore, the encoder output value e_n^U is given by the following $GF(2^N)$ equation:

$$e_n^U = 2 \cdot u_n^U + p_n = 2 \cdot u_n^U + x_{1n}^U \text{ mod } 2 \quad (1)$$

The trellis complexity of the codes generated with the scheme in Fig. 1 increases with the wordlength N , because the number of trellis states grows exponentially with the output wordlength, i.e., 2^N , while the number of transitions originating from and ending in the same state grows exponentially with the input wordlength, i.e., 2^{N-1} .

The set partitioning for the punctured TCM scheme, which optimizes the initialization of the a priori information for the first decoder, during the first iteration, was introduced in [6], and has two features. First of all, the set partitioning follows the Ungerboeck optimum set partitioning rules from [4], and secondly, the constellation points associated to the same group of $N - 1$ systematic information bits, i.e., to the same input symbol u_n^U , but differing in the least significant bit, i.e., the parity bit p_n , should be placed at the minimum distance in the set, $\Delta_{0,2^N\text{-ary modulation}}$. Following these two requirements, the optimum set partitioning rule for 16-QAM is depicted in Fig. 2. The first feature maximizes the minimum Euclidian distance of the component TCM code, while the second feature minimizes the distance between elements of the subsets associated to identical systematic bits, denoted by ovals in Fig. 2, for the global punctured TCM code.

It can be easily demonstrated that the minimum Euclidian distance for the 2^N -ary TCM component encoder presented in Fig. 1, using the properly partitioned constellations, has the following expression:

$$d_{E,R=\frac{N-1}{N}}^2 = \begin{cases} 2\Delta_{1,2^N\text{-PSK}}^2 + \Delta_{0,2^N\text{-PSK}}^2, & \text{for PSK} \\ 5\Delta_{0,2^N\text{-QAM}}^2, & \text{for QAM} \end{cases} \quad (2)$$

In Table I, some values of the minimum distance of the TCM encoder in Fig. 1 are presented for different values of N , and for the PSK and QAM constellations, respectively. The associated coding rates are presented in the second column. It can be easily noticed from (2) that all the rate

Table I
 MINIMUM 2^N -ARY TCM DISTANCES AS FUNCTION OF N FOR
 OPTIMUM GF(2^N) RSC-LCIRC ENCODERS.

N	R	Modulation	d_E^2	l'_m	d_p^2
2	1/2	QPSK, 4-QAM	10	3	32
3	2/3	8-PSK	≈ 4.5858	2	8
4	3/4	16-PSK	≈ 1.3238	2	≈ 1.1716
4	3/4	16-QAM	2	2	1.28

$(N - 1)/N$, for any N value, the RSC-LCIRC encoders have the same minimum distances as the corresponding binary optimum encoders [6], [7]. When transmitting over a Rayleigh non-selective fading channel the TCM system performances depend mainly on two parameters, i.e., the minimum effective length, and the minimum product distance [5]. We call the minimum effective length l_m the length of the shortest path pair of encoder output values (x_n, x'_n) . Among these paths of length l_m there is one having the smallest product distance $d_p^2 = \prod_{n=1}^{l_m} |x_n - x'_n|^2$. The values of these parameters are presented in the last two columns from Table I, for the same RSC-LCIRC codes. Again, the RSC-LCIRC encoders have the same values for minimum effective length and product distance, as their binary counterparts [5]. However, the GF(2^N) RSC-LCIRC encoders are less complex than the corresponding binary encoders in terms of memory usage. The memory size of the binary encoders increases logarithmically with the number of states in the trellis, while the GF(2^N) RSC-LCIRC encoders include only one delay element, no matter what the trellis complexity is. As another advantage of these encoders, we can also mention the Euclidian distance compact expression (2) as a function of N .

III. RSC-LCIRC ENCODER IN TURBO-TCM SCHEME

Fig. 3 shows the turbo TCM transmitter for 2^N -ary modulation. The information 2^{N-1} -ary symbol sequence u_n and its block-wise interleaved version $u_n^{(i)}$ are fed into two identical component encoders RSC-LCIRC₁ and RSC-LCIRC₂ of rate $(N - 1)/N$. The encoders' outputs are selected alternatively and mapped into 2^N -ary modulated symbol sequence x_n . The output of the bottom encoder is deinterleaved according to the inverse operation of the interleaver. This ensures that at the input of the symbol selector, the $N - 1$ information bits from the 2^{N-1} -ary input symbol, partly defining the encoded 2^N -ary symbols of both the upper and lower input, are identical [6], [7]. Therefore, if the selector is switched on a symbol base, the mapper output is a punctured version of the two encoded sequences, and the $N - 1$ information bits appear only once, mapped in a single transmitted symbol selected either from e_{1n} sequence or from e_{2n} sequence. Nevertheless, the remaining parity

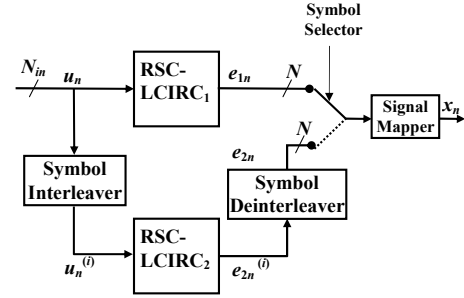


Figure 3. TCM transmitter with RSC-LCIRC encoders and symbol puncturing.

bit carried by the transmitted symbol is taken alternatively from the upper and lower encoder. Hence, the overall coding rate for the scheme in Fig. 3 is $(N - 1)/N$. The 2^N -levels modulated symbol sequence is transmitted over a noisy and non-selective fading channel. The received signal over the n -th symbol interval is given by:

$$y_n = h_n x_n + w_n \quad (3)$$

where w_n is an AWGN sequence with $E[|w_n|^2] = N_0$, and x_n denotes the 2^N -levels symbol value mapped from the encoders output sequences (e_{1n}, e_{2n}) by puncturing over the n -th symbol interval. The coefficient h_n is the path gain from transmit antenna to receive antenna, having a Rayleigh distribution. The path gains are modeled as the absolute part of samples of independent complex Gaussian random variables with variance 0.5 per real dimension. The wireless channel is assumed to be quasistatic, i.e., the path gain value is constant over a group of symbol intervals, and varies from one group of symbols to another. The receiver structure including two component decoders that use the symbol-by-symbol log-MAP algorithm was introduced in [6]. The decoding process is similar to the binary turbo decoding, except that the symbol probability is used as the extrinsic information rather than the bit probability [6], [7]. The log-MAP decoder computes the log likelihood ratio (LLR) for each group of information bits transmitted at the n -th symbol interval u_n , embedded in the 2^{N-1} -ary input symbol taking one of the integer values $j \in \{0, 1, \dots, 2^{N-1} - 1\}$ as [7]

$$L(u_n = j) = \ln \frac{P(u_n = j | \mathbf{y})}{P(u_n = 0 | \mathbf{y})} \quad (4)$$

where \mathbf{y} is the received signal vector. The symbol-by-symbol log-MAP decoder operates on an L symbols block basis. Hence, in all equations the symbol time variable n takes values between 1 and L . We assume that the receiver has perfect side information on the path gains (h_n) . The input symbol j with the largest LLR in (4) is chosen as the hard decision output.

A very important tool for the iterative decoding performances analysis consists in the EXIT chart, which de-

scribes the extrinsic mutual information exchange between constituent decoders. A complexity efficient method for generating the symbol-based EXIT charts from symbol-based a posteriori probabilities (APPs) was proposed in [11]. The expression for the average extrinsic information $I_E(u)$, estimated at the output of the decoder for the input symbol vector u , is given by [11]:

$$I_{E,D}(u) = N - 1 + \frac{1}{L} \sum_{n=1}^L \mathbf{E} \left[\sum_{i=1}^{2^{N-1}} e_D(u_n^{(i)}) \cdot \log_2(e_D(u_n^{(i)})) \right] \quad (5)$$

where L is the number of information symbols in the decoded block, $N - 1$ is the number of information bits per input symbol, $u_n^{(i)}$ is the presumed transmitted information symbol at time instant n for $i \in \{1, 2, \dots, 2^{N-1}\}$, and $e(\cdot)$ is the extrinsic probability. The expectation $\mathbf{E}[\cdot]$ can be approximated by simple time-averaging of the extrinsic probabilities of the information symbol. We propose to approximate the extrinsic probability as the normalized joint extrinsic and systematic information of the log-MAP decoder:

$$e_D(u_n^{(i)}) \approx \frac{\exp(L_{D,es}(u_n = i))}{\sum_{i=1}^{2^{N-1}} \exp(L_{D,es}(u_n = i))} \quad (6)$$

In equations (5) and (6), D denotes the decoder number, i.e., $D \in \{1, 2\}$. On the other hand, computing an exact value of the extrinsic probability requires that the systematic and parity parts of the channel observation variables are independent. Thus, equation (6) represents only an approximation of the true extrinsic information. The average a priori information $I_A(u)$ is computed in a similar manner. The EXIT chart is obtained by representing, on the same diagram, the decoder 1 transfer characteristic, i.e., $I_{E,1} = T(I_{A,1})$, and the decoder 2 transfer characteristic, i.e., $I_{E,2} = T(I_{A,2})$, for a constant E_b/N_0 value. The axes of the decoder 2 transfer characteristic are swapped.

IV. SIMULATIONS RESULTS

The TTCM scheme presented in Section III using the RSC-LCIRC encoders presented in Section II was tested for 8-PSK and 16-QAM by means of simulations over an AWGN non-faded channel, and over an AWGN and non-selective fading channel, respectively. Both component encoders in the TTCM scheme are identical rate-2/3 RSC-LCIRC encoders for 8-PSK, and rate-3/4 for 16-QAM, respectively. The modulation is using the optimum set partitioning for the punctured TTCM scheme as presented in Section II. The symbol interleavers used for simulations are pseudo-random and operate independently on even and odd positions [6]. The symbol-by-symbol log-MAP decoding algorithm is used in the receiver. The decoding convergence is investigated for several E_b/N_0 values, where E_b is the signal energy per bit and N_0 is one-sided power spectral density of the AWGN noise. The interleaver block includes 1024 symbols. As references, we considered the

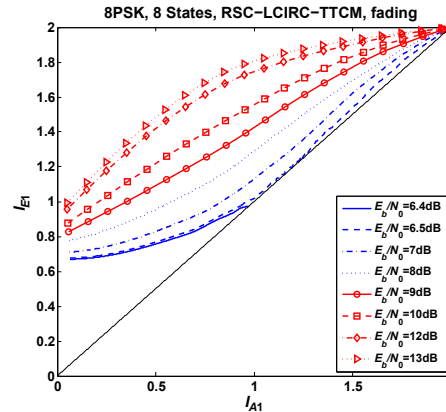


Figure 4. Extrinsic information transfer characteristic of 8PSK-RSC-LCIRC-TTCM decoder for a fading channel.

corresponding optimum binary encoders. Therefore, for rate-2/3 8-PSK TTCM scheme the optimum binary encoder with 8 states is given by the generator polynomials, represented in octal notation [11, 02, 04] [6]. The rate-3/4 optimum binary encoder with 16 states, considered as reference, was determined in [7] for 16-QAM TTCM with the generator polynomials [23, 35, 33, 37]. In the following, EXIT charts are contrived for 8PSK and 16QAM schemes presented above, using a simulation procedure described in [11]. These EXIT charts are relevant for the TTCM decoder convergence analysis, revealing important features, such as BER turbo cliff and BER floor regions. The average extrinsic information $I_E(u)$ and the average a priori information $I_A(u)$ are estimated using equation (5), assuming that the extrinsic probability is approximated with (6). Fig. 4 shows the extrinsic information transfer characteristic of 8PSK-RSC-LCIRC-TTCM decoder for a fading channel, assuming a variable E_b/N_0 . The considered scenario assumes the transmission over a non-selective Rayleigh fading channel, LCIRC encoded 8PSK TTCM scheme, and a blocklength of 2^{14} symbols. Analyzing the curves in Fig. 4 one can easily notice that above $E_b/N_0 = 6.4$ dB, the average decoding trajectory obtained from real simulations shows convergence. In Fig. 5(a), the EXIT chart for $E_b/N_0 = 6.5$ dB is depicted. This EXIT chart plots the *bottleneck region* with the decoding trajectory just managing to pass through a narrow tunnel, which corresponds to the BER waterfall region. In Fig. 5(a), the convergence is almost reached after 30 iterations. The EXIT chart obtained under the same assumptions, for the corresponding binary encoder, is plotted in Fig. 5(b). It is clear that for the binary case decoder the trajectory gets stuck as compared to the LCIRC decoder, for $E_b/N_0 = 6.5$ dB, assuming the same number of iterations. In Fig. 5(c) the EXIT chart corresponding to the *wide-open region* is depicted. The scenario is identical to the previous one, but for $E_b/N_0 = 13$ dB. This region is related to

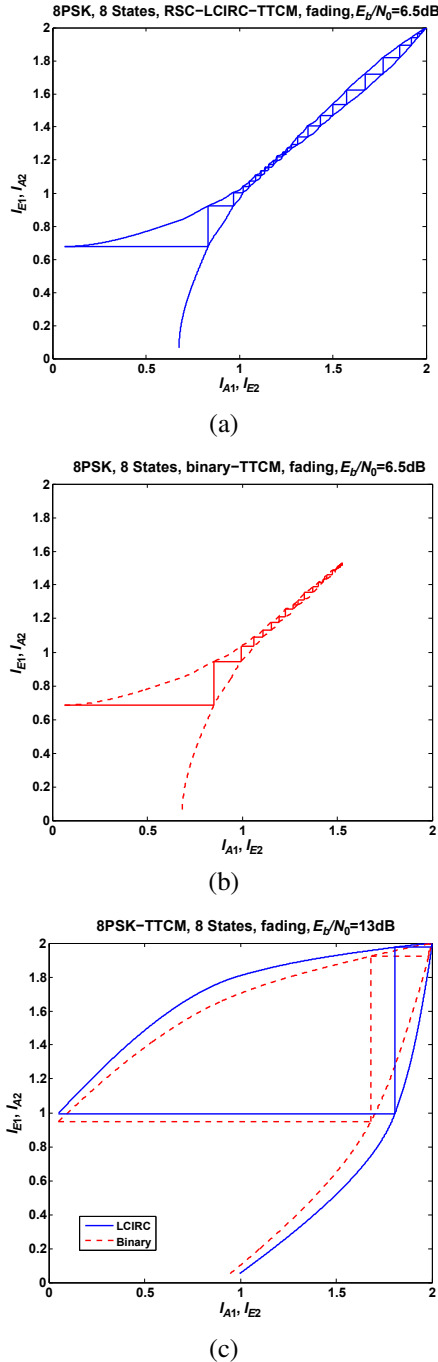


Figure 5. EXIT charts for 8PSK-TTCM over a fading channel. (a) LCIRC, $E_b/N_0 = 6.5$ dB; (b) Binary, $E_b/N_0 = 6.5$ dB; (c) $E_b/N_0 = 13$ dB.

the BER floor region. The trajectories for both binary and LCIRC decoders are depicted in Fig. 5(c). Again, the LCIRC decoder outperforms its binary counterpart due to the wider opening of the EXIT chart. In this case, the convergence is almost reached after 3 iterations.

Fig. 6 shows the extrinsic information transfer charac-

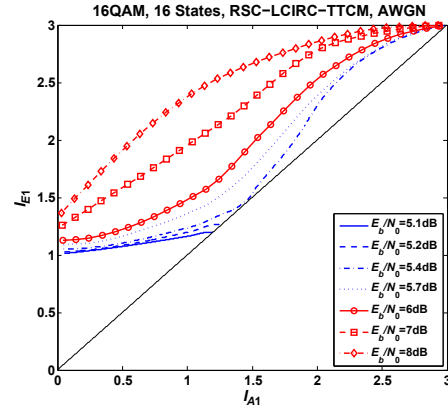


Figure 6. Extrinsic information transfer characteristic of 16QAM-RSC-LCIRC-TTCM decoder for a non-fading channel.

teristic of 16QAM-RSC-LCIRC-TTCM decoder for a non-fading channel, assuming a variable E_b/N_0 . A blocklength of 2^{14} symbols was considered. Analyzing the curves in Fig. 6, one can easily notice that above $E_b/N_0 = 5.4$ dB, the average decoding trajectory shows convergence. In Fig. 7(a), the EXIT chart for $E_b/N_0 = 5.4$ dB is depicted. This EXIT chart plots the *bottleneck region*, which corresponds to the BER waterfall region. In Fig. 7(a), the convergence is almost reached after 10 iterations. The EXIT chart obtained under the same assumptions, for the corresponding binary encoder, is plotted in Fig. 7(b). It is clear that for the binary case decoder, the trajectory is better than the LCIRC decoder one. In fact, the binary decoder needs less iterations (only 7) to converge, and the EXIT diagram is wider. In Fig. 7(c) the EXIT chart for $E_b/N_0 = 6$ dB, corresponding to the *wide-open region*, is depicted. In this case, the LCIRC decoder outperforms its binary counterpart, due to the wider opening of the EXIT chart. Moreover, the convergence is almost reached after 4 iterations. As a conclusion, the LCIRC outperforms the binary case for $E_b/N_0 > 5.8$ dB, while the opposite happens for lower values of E_b/N_0 .

V. CONCLUSION

It was demonstrated that using the LCIRC function, efficient RSC encoders over $GF(2^N)$ can be designed for punctured TTCM transmissions. A generalized 1-delay $GF(2^N)$ RSC encoder scheme using LCIRC was defined, for any possible encoding rate of $(N - 1)/N$. It was shown that LCIRC-based encoders offer at least the same performances as conventional binary encoders for the rate- $(N - 1)/N$ schemes. EXIT charts were provided to demonstrate their convergence properties. In perspective, we intend to extend the $GF(2^N)$ RSC encoders design using different nonlinear functions.

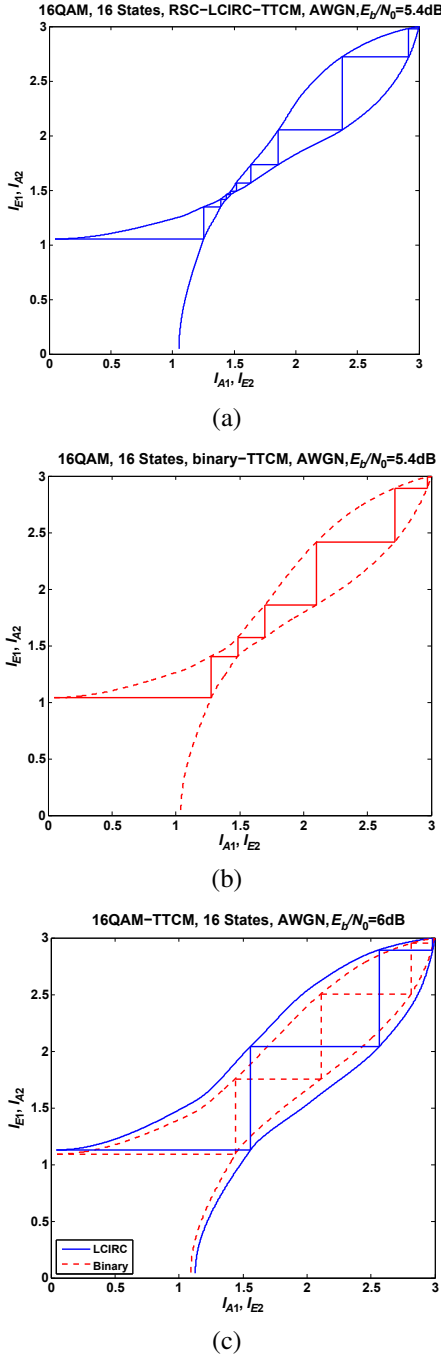


Figure 7. EXIT charts for 16QAM-TTCM over a non-fading channel. (a) LCIRC, $E_b/N_0 = 5.4$ dB; (b) Binary, $E_b/N_0 = 5.4$ dB; (c) $E_b/N_0 = 6$ dB.

ACKNOWLEDGMENT

This work was supported in part by the Romanian contract POSDRU/89/1.5/S/62557 and by the Romanian UEFISCSU PN-2 RU-TE Project no. 18/12.08.2010.

REFERENCES

- [1] D. R. Frey, "Chaotic digital encoding: An approach to secure communication," *IEEE Trans. Circuits and Systems - II: Analog and Digital Signal Processing*, vol. 40, pp. 660-666, Oct. 1993.
- [2] C. Vladeanu, S. El Assad, J.-C. Carlach, and R. Quéré, "Improved Frey Chaotic Digital Encoder for Trellis-Coded Modulation," *IEEE Trans. Circuits and Systems - II*, vol. 56, pp. 509-513, Jun. 2009.
- [3] C. Vladeanu, S. El Assad, J.-C. Carlach, R. Quéré, I. Marghescu, "Recursive $GF(2^N)$ Encoders Using Left-Circulate Function for Optimum PSK-TCM Schemes," *Signal Processing*, vol. 90, pp. 2708-2713, Sep. 2010.
- [4] G. Ungerboeck, "Channel coding with multilevel/phase signals," *IEEE Trans. Information Theory*, vol. IT-28, pp. 55-67, Jan. 1982.
- [5] C. Schlegel and D.J. Costello, "Bandwidth Efficient Coding for Fading Channels: Code Construction and Performance Analysis," *IEEE Trans. on Sel. Areas in Comm.*, vol. 7, pp. 1356-1368, Dec. 1989.
- [6] P. Robertson and T. Wozz, "Bandwidth-Efficient Turbo Trellis-Coded Modulation using Punctured Component Codes," *IEEE Trans. on Sel. Areas in Comm.*, vol. 16, pp. 206-218, Feb. 2000.
- [7] B. Vucetic and J. Yuan, "Turbo Codes: Principles and Applications," Springer, 2000.
- [8] C. Vladeanu and S. El Assad, "Punctured 8-PSK Turbo-TCM Transmissions Using Recursive Systematic Convolutional $GF(2^N)$ Encoders," in *Proc. 19th European Signal Conf. - EUSIPCO 2011*, Barcelona, Spain, Aug. 29 - Sept. 2, 2011, pp. 111-115.
- [9] S. ten Brink, "Convergence Behavior of Iteratively Decoded Parallel Concatenated Codes," *IEEE Trans. on Comm.*, vol. 49, pp. 1727-1737, Oct. 2001.
- [10] H. Chen and A. Haimovich, "EXIT Charts for Turbo Trellis-Coded Modulation," *IEEE IEEE Commun. Lett.*, vol. 8, pp. 668-670, Nov. 2004.
- [11] J. Kliewer, S. X. Ng, and L. Hanzo, "Efficient Computation of EXIT Functions for Nonbinary Iterative Decoding," *IEEE Trans. on Comm.*, vol. 54, pp. 2133-2136, Dec. 2006.
- [12] Soon Xin Ng, O.R. Alamri, Li Yonghui, J. Kliewer, L. Hanzo, "Near-Capacity Turbo Trellis Coded Modulation Design Based on EXIT Charts and Union Bounds," *IEEE Trans. on Comm.*, vol. 56, pp. 2030-2039, Dec. 2008.